ILCs can be replenished and complemented, albeit only in part, through contributions of hematogenously derived precursors or mature cells in situations of extended inflammation and tissue repair. Consistent with our findings, it has been reported that ILC subsets are elevated in the peripheral blood of patients suffering from psoriasis (*30*, *31*). Furthermore, peripheral blood ILC2s have been shown to dynamically modulate the expression of molecules that regulate tissue homing in mice and humans (*20*, *32*). In addition, we have detected donor-derived lymphoid and ILC progenitors in parabiotic BM (fig. S8), raising the possibility that ILC progenitors can physiologically seed tissues not only during embryonic development (*3*) but also in adult mice. It remains to be determined whether this observation reflects the physiologic migration of ILC progenitors or the engraftment of donor-derived hematopoietic stem cells (*33*, *34*) giving rise to ILCs. Independent of these considerations, our data support a model in which ILCs are locally maintained and expanded as tissue-resident cells during homeostasis and acute infection. This "sedentary" lifestyle of ILCs in broadly differing microenvironments is consistent with the proposed roles of ILCs as sentinels and local keepers of tissue function.

REFERENCES AND NOTES

1. D. Artis, H. Spits, *Nature* **517**, 293–301 (2015).
2. G. Eberl, M. Colonna, J. P. Di Santo, A. N. McKenzie, *Science* **348**, aaa6566 (2015).
3. J. K. Bando, H. E. Liang, R. M. Locksley, *Nat. Immunol.* **16**, 153–160 (2015).
4. E. Montaldo *et al.*, *Immunity* **41**, 988–1000 (2014).
5. M. G. Constantinides, B. D. McDonald, P. A. Verhoef, A. Bendelac, *Nature* **508**, 397–401 (2014).
6. C. S. Klose *et al.*, *Cell* **157**, 340–356 (2014).
7. R. A. Franklin *et al.*, *Science* **344**, 921–925 (2014).
8. P. Kamran *et al.*, *J. Vis. Exp.* **2013**, e50556 (2013).
9. H. Peng *et al.*, *J. Clin. Invest.* **123**, 1444–1456 (2013).
10. K. G. Anderson *et al.*, *Nat. Protoc.* **9**, 209–222 (2014).
11. M. H. Kim, E. J. Taparowsky, C. H. Kim, *Immunity* **43**, 107–119 (2015).
12. C. C. Bain *et al.*, *Nat. Immunol.* **15**, 929–937 (2014).
13. E. C. Mackley *et al.*, *Nat. Commun.* **6**, 5862 (2015).
14. D. K. Sojka *et al.*, *eLife* **3**, e01659 (2014).
15. J. M. Kim, J. P. Rasmussen, A. Y. Rudensky, *Nat. Immunol.* **8**, 191–197 (2007).
16. K. Liu *et al.*, *Science* **324**, 392–397 (2009).
17. M. Camberis, G. Le Gros, J. Urban Jr., *Curr. Protoc. Immunol.* (2003).
18. Y. Huang *et al.*, *Nat. Immunol.* **16**, 161–169 (2015).
19. B. J. Marsland, M. Kurrer, R. Reissmann, N. L. Harris, M. Kopf, *Eur. J. Immunol.* **38**, 479–488 (2008).
20. E. D. Tait Wojno *et al.*, *Mucosal Immunol.* (2015).
21. J. E. Turner *et al.*, *J. Exp. Med.* **210**, 2951–2965 (2013).
22. G. Gasteiger, A. Y. Rudensky, *Nat. Rev. Immunol.* **14**, 631–639 (2014).
23. G. Gasteiger, S. Hemmers, P. D. Bos, J. C. Sun, A. Y. Rudensky, *J. Exp. Med.* **210**, 1179–1187 (2013).
24. B. Roediger *et al.*, *J. Allergy Clin. Immunol.* (2015).
25. C. Wilhelm *et al.*, *Nat. Immunol.* **12**, 1071–1077 (2011).
26. A. B. Molofsky *et al.*, *Immunity* **43**, 161–174 (2015).
27. C. Vonarbourg *et al.*, *Immunity* **33**, 736–751 (2010).
28. J. H. Bernink *et al.*, *Immunity* **43**, 146–160 (2015).
29. S. A. van de Pavert *et al.*, *Nature* **508**, 123–127 (2014).
30. M. B. Teunissen *et al.*, *J. Invest. Dermatol.* **134**, 2351–2360 (2014).
31. F. Villanova *et al.*, *J. Invest. Dermatol.* **134**, 984–991 (2014).
32. J. M. Mjösberg *et al.*, *Nat. Immunol.* **12**, 1055–1062 (2011).
33. D. E. Wright, A. J. Wagers, A. P. Gulati, F. L. Johnson, I. L. Weissman, *Science* **294**, 1933–1936 (2001).
34. J. L. Abkowitz, A. E. Robinson, S. Kale, M. W. Long, J. Chen, *Blood* **102**, 1249–1253 (2003).

ACKNOWLEDGMENTS

We thank R. Franklin, S. Dadi, M. Li, and A. Chaudhry for help with parabiosis or cell isolations; D. Artis, L. Monticelli, and B. Hoyos for providing and maintaining worms; K. Wu and A. Bravo for general laboratory support; and T. O'Sullivan, J. Sun, A. Diefenbach, W. Kastenmüller, and members of the Rudensky and Gasteiger laboratories for critical discussions. Data from this study are tabulated in the main paper or in the supplementary materials. This work was supported by an Irvington Fellowship from the Cancer Research Institute (G.G.), NIH Medical Scientist Training Program grant T32GM07739 to the Weill Cornell/Rockefeller/Sloan-Kettering Tri-Institutional MD-PhD Program (X.F.), Cancer Center Support Grant P30CA008748 from the NIH National Cancer Institute, NIH grant R37AI034206 (A.Y.R.), the Ludwig Center at Memorial Sloan Kettering Cancer Center, and the Hilton-Ludwig Cancer Prevention Initiative (Conrad N. Hilton Foundation and Ludwig Cancer Research) (A.Y.R.). G.G. is an investigator with the Deutsche Forschungsgemeinschaft Emmy Noether Programme, and A.Y.R is an investigator with the Howard Hughes Medical Institute.

SUPPLEMENTARY MATERIALS

www.sciencemag.org/content/350/6263/981/suppl/DC1
Materials and Methods
Figs. S1 to S8

5 July 2015; accepted 2 October 2015
Published online 15 October 2015
10.1126/science.aac9593

CANCER IMMUNOLOGY

Patrolling monocytes control tumor metastasis to the lung

Richard N. Hanna,[1]* Caglar Cekic,[2] Duygu Sag,[3] Robert Tacke,[1] Graham D. Thomas,[1] Heba Nowyhed,[1] Erica Herrley,[1] Nicole Rasquinha,[1] Sara McArdle,[4] Runpei Wu,[1] Esther Peluso,[1] Daniel Metzger,[5] Hiroshi Ichinose,[6] Iftach Shaked,[1] Grzegorz Chodaczek,[4] Subhra K. Biswas,[7] Catherine C. Hedrick[1]*

The immune system plays an important role in regulating tumor growth and metastasis. Classical monocytes promote tumorigenesis and cancer metastasis, but how nonclassical "patrolling" monocytes (PMo) interact with tumors is unknown. Here we show that PMo are enriched in the microvasculature of the lung and reduce tumor metastasis to lung in multiple mouse metastatic tumor models. Nr4a1-deficient mice, which specifically lack PMo, showed increased lung metastasis in vivo. Transfer of Nr4a1-proficient PMo into Nr4a1-deficient mice prevented tumor invasion in the lung. PMo established early interactions with metastasizing tumor cells, scavenged tumor material from the lung vasculature, and promoted natural killer cell recruitment and activation. Thus, PMo contribute to cancer immunosurveillance and may be targets for cancer immunotherapy.

Monocytes and monocyte-derived macrophages play key roles in tumor progression (*1*–*4*). Classical "inflammatory" monocytes ($CCR2^{high}Ly6C^{+}$ in mice; $CCR2^{high}CD14^{+}CD16^{-}$ in humans) are recruited to tumor sites where they contribute to macrophage content and promote growth and metastasis (*5*, *6*). In contrast, very little is known about the role of nonclassical "patrolling" monocytes (PMo) ($CX3CR1^{high}Ly6C^{-}$ in mice; $CX3CR1^{high}CD14^{dim}CD16^{+}$ in humans) in the early growth and metastasis of tumors. PMo are involved in the resolution of inflammation; they actively survey the endothelium of the vasculature, where they scavenge microparticles and remove cellular debris (*7*–*9*). The orphan nuclear receptor Nr4a1 (also known as Nur77/TR3/NGIFB) is highly expressed in PMo compared with other immune cells and functions as a master regulator for the development of PMo in mice (*10*).

To investigate the actions of PMo during early tumor metastasis, we used mice expressing green fluorescent protein (GFP) under the control of the Nr4a1 promoter (Nr4a1-GFP mice). In these mice, PMo (but not $Ly6C^{+}$ classical monocytes) express high levels of GFP (GFP^{high}) (*10*, *11*). We focused our studies on the lung, which is a common site of tumor metastasis and an important locus of PMo activity (*12*–*14*). We used flow cytometry to confirm that Nr4a1-GFP^{high} cells in the lung were PMo (fig. S1, A to C). Tracking of Nr4a1-GFP^{high} cells by confocal imaging in the lungs allowed us to identify a large number of Nr4a1-GFP^{high} PMo patrolling the microvasculature (movie S1 and Fig. 1A). Consistent with an important role for PMo in the lung vasculature, we found a three- to fourfold enrichment of Nr4a1-GFP^{high} PMo in the lung compared with other tissues (fig. S1D).

To examine the interactions of PMo with tumors in vivo, we imaged Nr4a1-GFP^{high} PMo in the lung after intravenous (IV) injection of Lewis

[1]Division of Inflammation Biology, La Jolla Institute for Allergy and Immunology, La Jolla, CA 92037, USA. [2]Department of Molecular Biology and Genetics, Bilkent University, Ankara, Turkey. [3]Izmir Biomedicine and Genome Center, Dokuz Eylul University, Izmir, Turkey. [4]Microscopy Core, La Jolla Institute for Allergy and Immunology, La Jolla, CA 92037, USA. [5]Department of Functional Genomics and Cancer, Institut de Génétique et de Biologie Moléculaire et Cellulaire (IGBMC), INSERM U964, CNRS UMR 7104, Université de Strasbourg, Illkirch, France. [6]Graduate School of Bioscience and Biotechnology, Tokyo Institute of Technology, Yokohama, Japan. [7]Singapore Immunology Network (SIgN), Agency for Science, Technology and Research (A*STAR), Singapore.
*Corresponding author. E-mail: rhanna@lji.org (R.N.H.); hedrick@lji.org (C.C.H.)

lung carcinoma cells expressing red fluorescent protein (LLC-RFP). The number of Nr4a1-GFP^{high} monocytes in the lung increased significantly 24 hours after injection, which implies that PMo are actively recruited to the lung tumor environment (Fig. 1A). Within 4 hours after tumor injection, most Nr4a1-GFP^{high} monocytes exhibited decreased patrolling speed in the vasculature, and by 24 hours they had arrested near lung tumor sites (Fig. 1B). The majority of Nr4a1-GFP^{high} monocytes isolated from the lung after LLC tumor transfer maintained their PMo phenotype, which we further confirmed in vitro (Fig. 1C and fig. S1).

Nr4a1-GFP^{high} PMo were recruited to tumor cell clusters within 30 min after IV tumor injection, and recruitment continued for at least 7 days (Fig. 1, D and E, and movies S2 to S5). Nr4a1-GFP^{high} cells that were recruited to lung tumor sites were not positive for Ly6C/G (GR-1) in vivo, further confirming that these Nr4a1-GFP^{high} cells are not Ly6G$^+$ granulocytes or Ly6C$^+$ classical monocytes (movie S4). The kinetics of PMo recruitment to the lung differed from that of Ly6C$^+$ monocytes (fig. S2A). At 7 days, there were significantly higher numbers of Nr4a1-GFP^{high} PMo (~24/100 μm^3) associated with tumor areas compared with tumor-free areas, confirming active recruitment of PMo to the tumor (Fig. 1, D and E; movie S5; and fig. S1B).

Nr4a1-GFP^{high} monocytes patrolling the vasculature 4 hours after tumor injection appeared to move toward and inhibit the attachment of tumor cells to the lung microvasculature (movie S3). We examined whether Nr4a1-GFP^{high} PMo could extravasate outside the vasculature. We found that by 4 hours after tumor injection, 10 to 20% of Nr4a1-GFP^{high} PMo had extravasated at tumor sites (fig. S2, B and C), and this increased to 40 to 50% PMo extravasation by 7 days. Together, these findings confirm that PMo establish early immune interactions with tumor cells and can extravasate and accumulate at tumor sites.

To determine whether PMo have a major role in regulating tumor invasion, metastasis, and growth in the lungs in vivo, we used Nr4a1 knockout (*Nr4a1*$^{-/-}$) mice, which exhibit selective loss of PMo (*10*) (fig. S3). *Nr4a1*$^{-/-}$ mice were IV injected with either syngeneic B16F10 melanoma cells expressing a luciferase reporter or LLC-RFP cells (Fig. 2, A and B, and figs. S4 and S5). As early as 24 hours and up to 21 days after IV injection of B16F10 melanoma, we observed increased tumor invasion in the lungs of *Nr4a1*$^{-/-}$ mice compared with control mice (Fig. 2, A and B, and fig. S4, A and B). We observed no differences in either Ly6C$^+$ monocyte or Ly6G$^+$ granulocyte populations in the lungs of these mice 7 days after tumor injection (fig. S4C). B16F10 tumor invasion appeared to be specific for the lung, as increased tumor metastasis was not observed in the liver (fig S4B). Additionally, increased spontaneous metastases to the lung were observed in *Nr4a1*$^{-/-}$ mice after subcutaneous injection of B16F10 melanoma, which suggests that Nr4a1 expression is important for suppressing primary tumor metastasis to the lung (Fig. 2C). A similar early and sustained increase in lung metastasis in *Nr4a1*$^{-/-}$ mice was also observed after intravenous LLC tumor transfer (fig. S5). We did not detect differences in lung vascular permeability between *Nr4a1*$^{-/-}$ and control mice (fig. S6).

We next investigated the mouse mammary tumor virus–polyoma middle T (MMTV-PyMT) model, in which female mice spontaneously develop mammary tumors that metastasize to the lung (*15*). To focus on Nr4a1 function exclusively in hematopoietic cells, we performed bone marrow

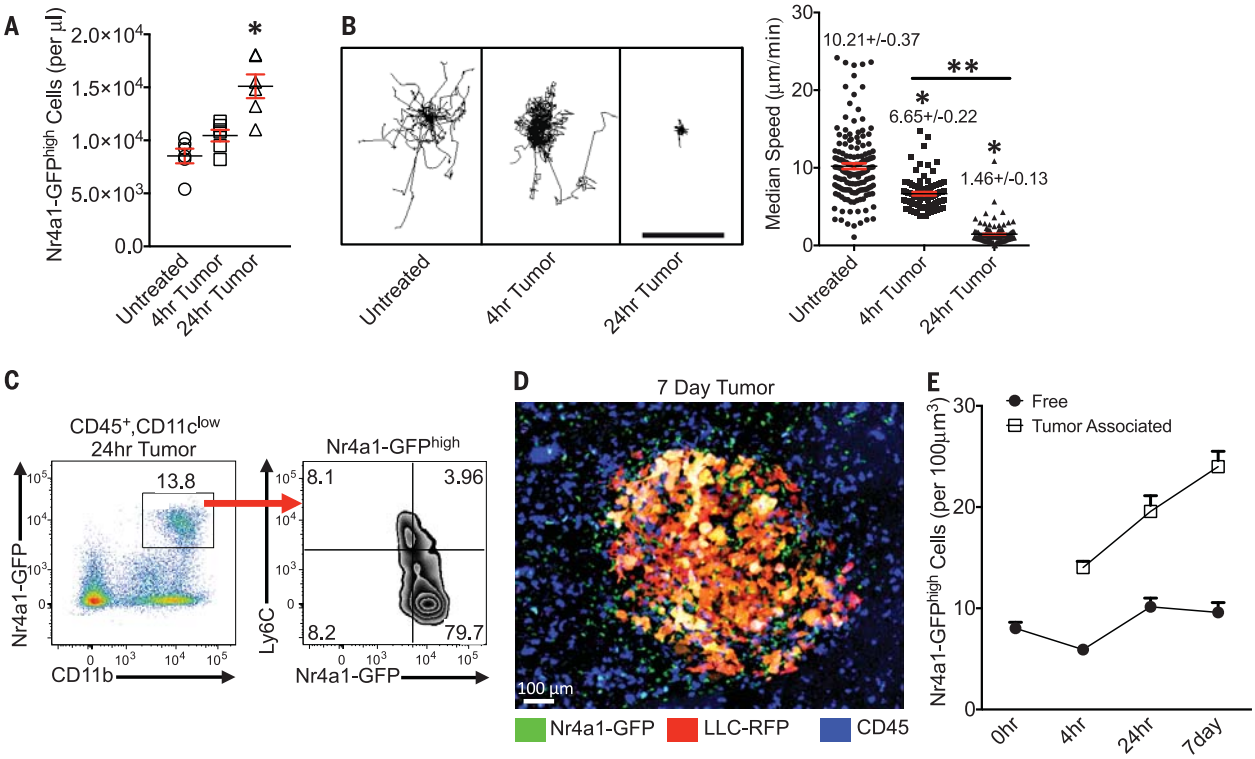

Fig. 1. Nr4a1-GFP^{high} monocytes patrol the vasculature and interact with tumor cells in the lung. (**A**) Quantification of Nr4a1-GFP^{high} PMo per microliter of blood volume in lung for control tissue (Untreated) or 4 or 24 hours after IV LLC-RFP transfer (n = 5 mice per group). (**B**) Quantification of Nr4a1-GFP^{high} monocyte movement in the lung before (Untreated), 4 hours after, or 24 hours after LLC-RFP tumor injection. (Left) Monocyte tracks transposed to a common origin from a representative 20-min movie (scale bar, 100 μm). (Right) Quantification of median speed of monocytes (combined speed data from analysis of three separate mice; *P < 0.001 lower than untreated; **P < 0.001 lower than 4-hour tumor). (**C**) Representative gating of Nr4a1-GFP^{high}CD11b$^+$ cells from all live CD45$^+$CD11c^{low} cells 24 hours after IV LLC-RFP transfer. (**D**) Representative confocal image of Nr4a1-GFP^{high} monocytes (green) interacting with LLC-RFP cells (red) in the lung 7 days after IV LLC-RFP transfer. Immune cells in the vasculature were labeled with IV-injected antibody to CD45 (blue). (**E**) Quantification of free (>100 μm from tumor site) and tumor-associated (<50 μm from tumor site) Nr4a1-GFP^{high} monocytes in the lung at various time points after tumor injection (combined analysis of five mice per group; P < 0.01 for each tumor-associated area compared with tumor-free areas for each time point). Error bars indicate SEM.

transplants using either wild-type (WT) or *Nr4a1*$^{-/-}$ bone marrow transferred into female recipient MMTV-PyMT mice. MMTV-PyMT mice receiving *Nr4a1*$^{-/-}$ bone marrow developed significantly higher numbers of spontaneous metastases to the lung but no differences in primary mammary tumor growth compared to mice receiving WT bone marrow (Fig. 2, D and E).

We further tested hematopoietic Nr4a1 function using B16F10 melanoma. Only mice receiving *Nr4a1*$^{-/-}$ bone marrow had increased B16F10 tumor metastases, confirming that Nr4a1 expression in hematopoietic cells regulated tumor cell metastasis to the lung (fig. S7, A and B). Analysis of immune cells isolated from lung tumors verified a selective loss of PMo in *Nr4a1*$^{-/-}$ bone marrow–transplanted mice (fig. S7C). In the 1:1 chimera mice, we observed equal reconstitution of immune cells from each donor (fig. S7D). However, PMo were derived almost exclusively from WT bone marrow, suggesting that the restoration of the Ly6C^{-} monocyte population prevented tumor metastasis.

To confirm that Nr4a1 expressed in myeloid cells was regulating tumor metastasis to the lung, we examined two different myeloid-specific Nr4a1 conditional knockout models (CSF1R-Cre^{+}*Nr4a1*$^{fl/fl}$ and LysM-Cre^{+}*Nr4a1*$^{fl/fl}$). Deletion of Nr4a1 using CSF1R-Cre^{+}*Nr4a1*$^{fl/fl}$ and LysM-Cre^{+}*Nr4a1*$^{fl/fl}$ mice significantly reduced the number of PMo in circulation (fig. S8) and increased tumor lung metastasis (Fig. 3, A and B, and fig. S9). Nr4a1 deletion using CSF1R-Cre or LysM-Cre also targets Nr4a1 in macrophages and Ly6C^{+} monocytes, so we cannot completely rule out effects of Nr4a1 in these cells. However, Nr4a1 expression in macrophages and Ly6C^{+} monocytes is relatively low, which suggests limited Nr4a1 function (*10*, *16*, *17*). No differences in tumor metastasis were observed with T lymphocyte–specific Nr4a1 deletion (fig. S10). Collectively, our studies illustrate increased lung metastasis burden in the absence of Nr4a1 in myeloid cells in multiple cancer models.

To confirm a direct role for PMo in regulating tumor metastasis, WT Ly6C^{+} or Ly6C^{-} monocytes were adoptively transferred into recipient *Nr4a1*$^{-/-}$ mice before tumor injection. A substantial number of the transferred monocytes could be found in the lungs (fig. S11, A and B). Reconstitution of PMo into *Nr4a1*$^{-/-}$ mice prevented lung tumor metastasis (Fig. 3, C and D). In contrast, transfer of Ly6C^{+} monocytes into *Nr4a1*$^{-/-}$ mice actually promoted tumor metastasis, consistent with known protumoral properties of this subset of monocytes (*5*, *18*). The majority (80 to 90%) of transferred Ly6C^{+} monocytes in circulation did not lose Ly6C expression (fig. S11C). Transfer of PMo 24 hours after tumor injection into *Nr4a1*$^{-/-}$ mice did not suppress tumor metastasis (fig. S11D), suggesting that PMo must already be present and active in the vasculature to prevent early tumor metastasis. These data directly show that nonclassical PMo inhibit tumor metastasis to the lung.

Patrolling monocytes can act as "intravascular housekeepers" that scavenge microparticles and remove cellular debris from the microvasculature (*7*). Extracellular vesicles from tumors are important mediators of tumor metastasis, progression, and immune suppression, and targeting their removal is an emerging focus for cancer therapy (*19*, *20*). We used high-resolution confocal imaging to determine whether PMo could engulf and remove tumor material from the lung vasculature. A sizable number of Nr4a1-GFP^{high} PMo containing large amounts of LLC-RFP tumor material were observed at tumor sites in the lung 24 hours after IV tumor transfer (Fig. 3E). Coculture assays of mouse PMo with fluorescently labeled tumor cells confirmed engulfment of large amounts of tumor material (Fig. 3F). Analysis of monocyte populations isolated from the lung at 24 hours after IV LLC-RFP injection indicated that PMo preferentially took up ~fivefold more tumor material than did Ly6C^{+} classical

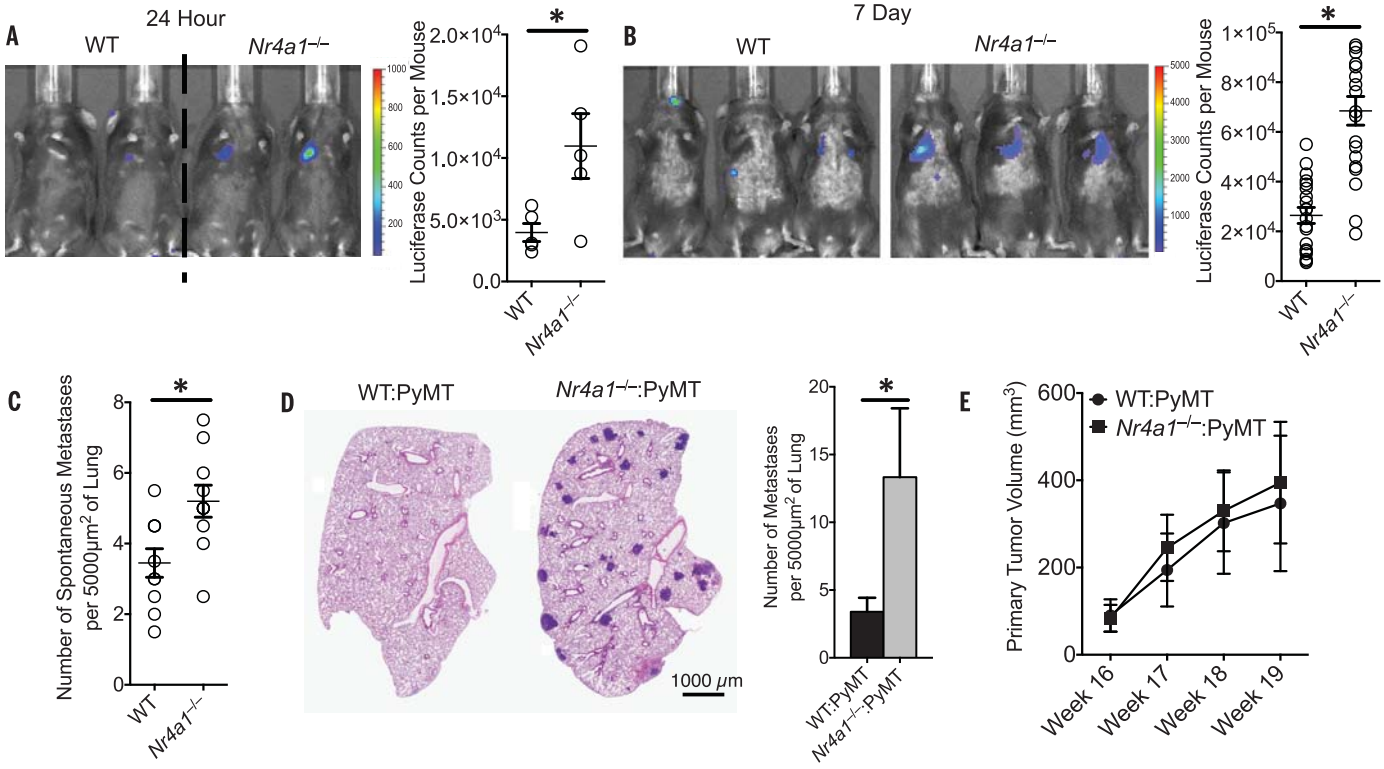

Fig. 2. Increased lung metastasis of tumors in *Nr4a1*$^{-/-}$ mice. (**A**) (Left) In vivo luciferase detection in WT control and *Nr4a1*$^{-/-}$ mice 24 hours after IV injection of 5 × 10^5 B16F10 melanoma cells expressing luciferase. (Right) Luciferase quantification (*P < 0.03, representative experiment with five mice per group). (**B**) In vivo luciferase detection (left) and quantification (right) in WT and *Nr4a1*$^{-/-}$ mice 7 days after IV injection with 3 × 10^5 B16F10-luciferase cells (*P < 0.001, n = 18 mice per group combined from three separate experiments). (**C**) Number of spontaneous tumor metastases per 5000 μm^2 of lung surface 28 days after subcutaneous injection of 1 × 10^5 B16F10-YFP cells (*P < 0.01, n = 7 mice per group). (**D** and **E**) Lung tumor metastasis in MMTV-PyMT mice reconstituted with WT (WT:PyMT) or *Nr4a1*$^{-/-}$ (*Nr4a1*$^{-/-}$:PyMT) bone marrow. (D) (Left) Representative MMTV-PyMT mouse lung histology, stained with hematoxylin and eosin. (Right) Quantification of the number of spontaneous lung metastases per 5000 μm^2 of lung surface (*P < 0.05, n = 12 for WT and 15 for *Nr4a1*$^{-/-}$). (E) Quantification of primary breast tumor growth in MMTV-PyMT mice (n = 12 for WT and 15 for *Nr4a1*$^{-/-}$). Error bars indicate SEM.

monocytes (Fig. 3G). PMo also preferentially took up substantially more B16F10–yellow fluorescent protein (YFP) tumor material, with an average tumor material size of 1.39 μm^2 and an average total amount of tumor material per monocyte of 1.92 μm^2 (fig. S12, A and B). The homologous human $CD14^{dim}CD16^+$ population of PMo, which similarly has high Nr4a1 expression (*8*, *21*), also engulfed a large quantity of tumor material in vitro, suggesting analogous tumor engulfment function (fig. S12C). Moreover, PMo actively engulfed tumor material within classic endocytic compartments (*22*) (Fig. 4A). Collectively, these results demonstrate that Nr4a1-dependent PMo rapidly and preferentially endocytose tumor material.

We then asked how PMo recognized tumor cells to prevent metastasis in the lung. The chemokine receptor CX3CR1 is highly expressed on PMo and is important for their arrest at inflammatory sites (fig. S13A) (*23*–*25*). CX3CR1-deficient (*Cx3cr1*$^{-/-}$) mice, which also have a significant reduction in PMo, exhibit a similar phenotype to *Nr4a1*$^{-/-}$ mice (i.e., increased tumor burden and metastasis to the lung) (*26*, *27*). Although PMo numbers were reduced in the lung vasculature of *Cx3cr1*$^{-/-}$mice [~30 to 50% reduction (fig. S13B), confirming previous reports] (*27*), a major proportion of the remaining CX3CR1-deficient PMo was observed patrolling the vasculature, as previously observed (*7*). Unlike *Cx3cr1*$^{-/+}$or WT PMo, *Cx3cr1*$^{-/-}$ PMo did not arrest near LLC tumor cells and instead remained patrolling within the lung vasculature (Fig. 4, B and C, and movie S6). *Cx3cr1*$^{-/-}$ PMo were not recruited to the lung 24 hours after LLC tumor challenge, whereas $Ly6C^+$ recruitment was unaffected by the loss of CX3CR1 expression (fig. S13B). *Cx3cr1*$^{-/-}$ PMo present in the lung showed defective engulfment of tumor material, indicating that CX3CR1 expression on PMo is critical for mediating the sensing and uptake of tumor material (Fig. 4D).

CX3CL1, a ligand for CX3CR1, has been reported to be present in high levels in human and mouse lungs (*28*). Using a CX3CL1-mCherry reporter mouse (*29*), we found that CX3CL1 was specifically expressed on $CD31^+$ endothelial cells (ECs) at low levels in the lung microvasculature (Fig. 4, E and F, and fig. S13C). CX3CL1 expression was most prevalent in lung ECs compared with ECs in other tissues (fig. S13D), which may partially explain the enrichment and preferential function of PMo in the lung. CX3CL1 expression on lung ECs increased in response to tumor challenge (Fig. 4E) and at sites of tumor metastasis (Fig. 4F), consistent with reports of increased CX3CL1 during lung inflammation (*30*).

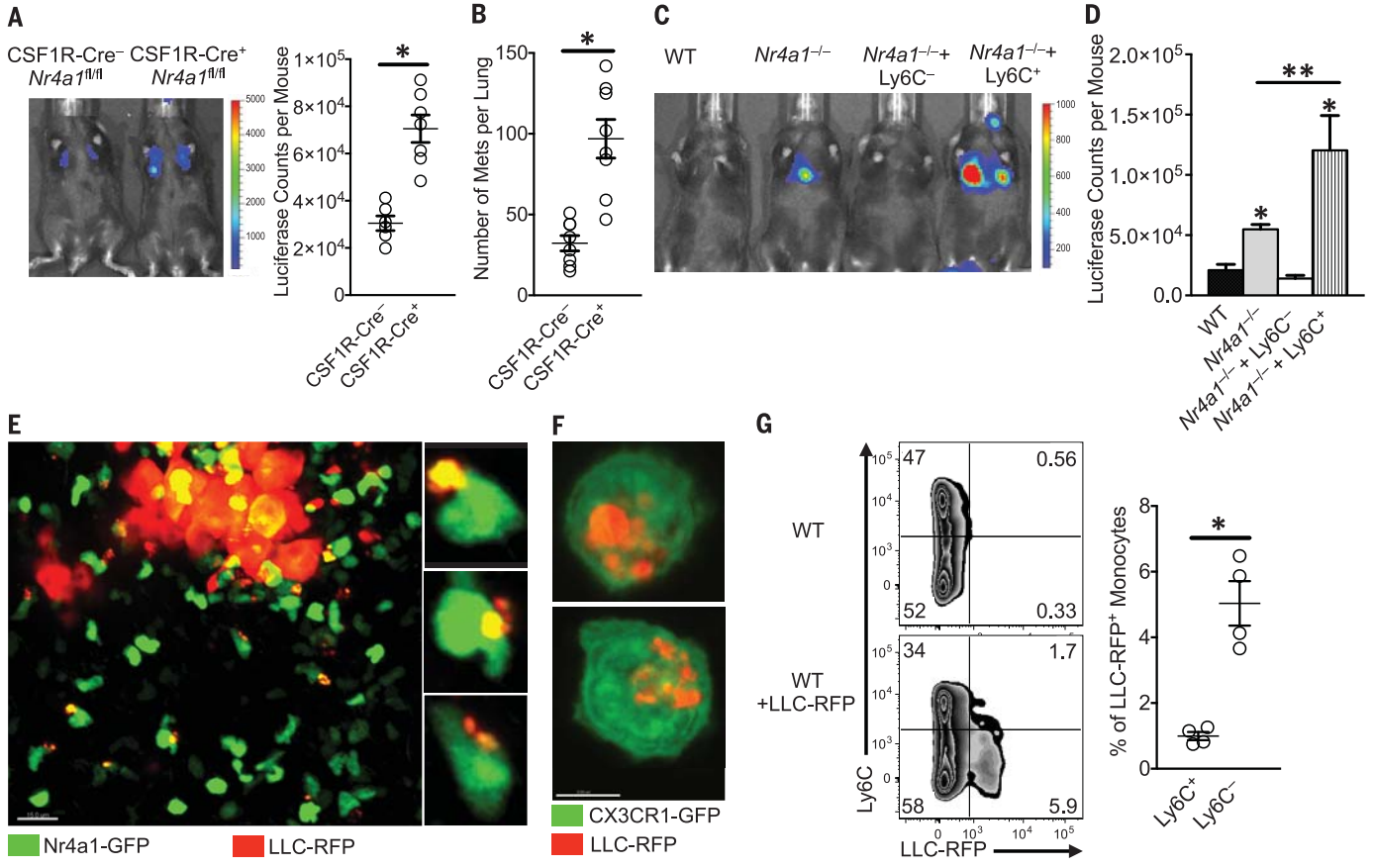

Fig. 3. Nr4a1-expressing PMo reduce tumor metastasis and engulf tumor material in the lung. (**A**) In vivo imaging (left) and quantification (right) of lung tumors in CSF1R-Cre$^-$*Nr4a1*$^{fl/fl}$ (CSF1R-Cre$^-$) or CSF1R-Cre$^+$*Nr4a1*$^{fl/fl}$ (CSF1R-Cre$^+$) mice 7 days after IV injection of 3 × 10^5 B16F10-luciferase tumor cells (n = 6 mice per group, *P < 0.01; experiment replicated twice). (**B**) Quantification of the number of tumor metastases per lung of CSF1R-Cre$^-$*Nr4a1*$^{fl/fl}$ (CSF1R-Cre$^-$) and CSF1R-Cre$^+$*Nr4a1*$^{fl/fl}$ (CSF1R-Cre$^+$) mice 7 days after IV injection of 3 × 10^5 B16F10-YFP tumor cells (n = 8 mice per group, *P < 0.01). (**C** and **D**) *Nr4a1*$^{-/-}$ mice were injected intravenously with 5 × 10^5 WT $Ly6C^-$ PMo, $Ly6C^+$ inflammatory monocytes, or PBS at day 0. On day 1, 3 × 10^5 B16F10-luciferase tumor cells were injected intravenously, and tumor metastasis and growth were measured by in vivo imaging on day 8. Shown are representative in vivo images (C) and quantification (D) of B16F10-luciferase metastasis 8 days after monocyte transfer and 7 days after tumor transfer in WT or *Nr4a1*$^{-/-}$ mice (combined data from five separate experiments with n = 2 mice per group; *P < 0.01 statistically different from WT; **P < 0.05 statistically different from *Nr4a1*$^{-/-}$). (**E**) Imaging of tumor material uptake in lung by Nr4a1-GFP^{high} monocytes 24 hours after IV injection of LLC-RFP tumor cells. Representative higher-magnification images are shown at right. Note that Nr4a1-GFP expression is primarily nuclear, so monocyte cell membranes are not visible in these images. (**F**) Uptake of LLC-RFP tumor material by CX3CR1-GFP$^{high}Ly6C^-$ PMo after 24 hours of coculture. (**G**) Representative flow plot (left) and quantification (right) of tumor material uptake by all monocytes in the lung 24 hours after IV tumor injection of 3 × 10^5 LLC-RFP cells (n = 4 mice per group; *P < 0.01; experiment replicated three times). Error bars indicate SEM.

Toll-like receptor 7 (TLR7) has been linked to recruitment of PMo in response to kidney damage in mice (*7*). However, we found that TLR7 did not play a major role in either recruitment of PMo to the lung after tumor injection (fig. S13B) or uptake of tumor material by PMo (Fig. 4D). We conclude that both CX3CR1 expression on monocytes and CX3CL1 expression by ECs are critical for recruitment of PMo to sites of tumor extravasation to mediate the removal of tumor material from the lung. CX3CL1 expression by tumor cells (*31*) may also drive monocyte recruitment. In agreement with our findings, many studies have reported that CX3CL1 expression by either tumor cells or tumor-associated cells is anti-tumoral and correlated with good prognosis (*32*–*34*). However, the function of the CX3CL1/CX3CR1 axis, particularly during later stages of tumor growth, is complex (*35*, *36*).

Finally, we examined whether PMo can directly kill tumor cells. After multiple attempts using various experimental conditions, direct killing of tumor cells by PMo was not observed (fig. S14). However, PMo may be important for antibody-dependent cell-mediated cytotoxicity of either tumor cells or suppressive immune cells within the tumor environment (*37*, *38*). In response to IV-injected B16F10 tumor, PMo isolated from lungs produced significantly higher levels of natural killer (NK) cell activation and recruitment-related chemokines CCL3, CCL4, and CCL5, as compared with classical Ly6C$^+$ monocytes (Fig. 4G) (*39*, *40*). In accord with this finding, myeloid-specific Nr4a1 knockout mice (CSF1R-Cre$^+$*Nr4a1*$^{fl/fl}$) showed reduced NK cell recruitment to the lung in response to tumor (Fig. 4H), suggesting that PMo controlled the recruitment of NK cells to tumor sites. A similar reduction in NK cell recruitment and CD44 activation (fig. S15, A and B) was also observed in the lungs of PyMT mice that received Nr4a1-deficient bone marrow. However, Nr4a1 does not regulate NK cell development (fig. S15C). Uptake of tumor material by PMo does not require the presence of NK cells (fig. S16, A and B). NK cell depletion reduced the differences in

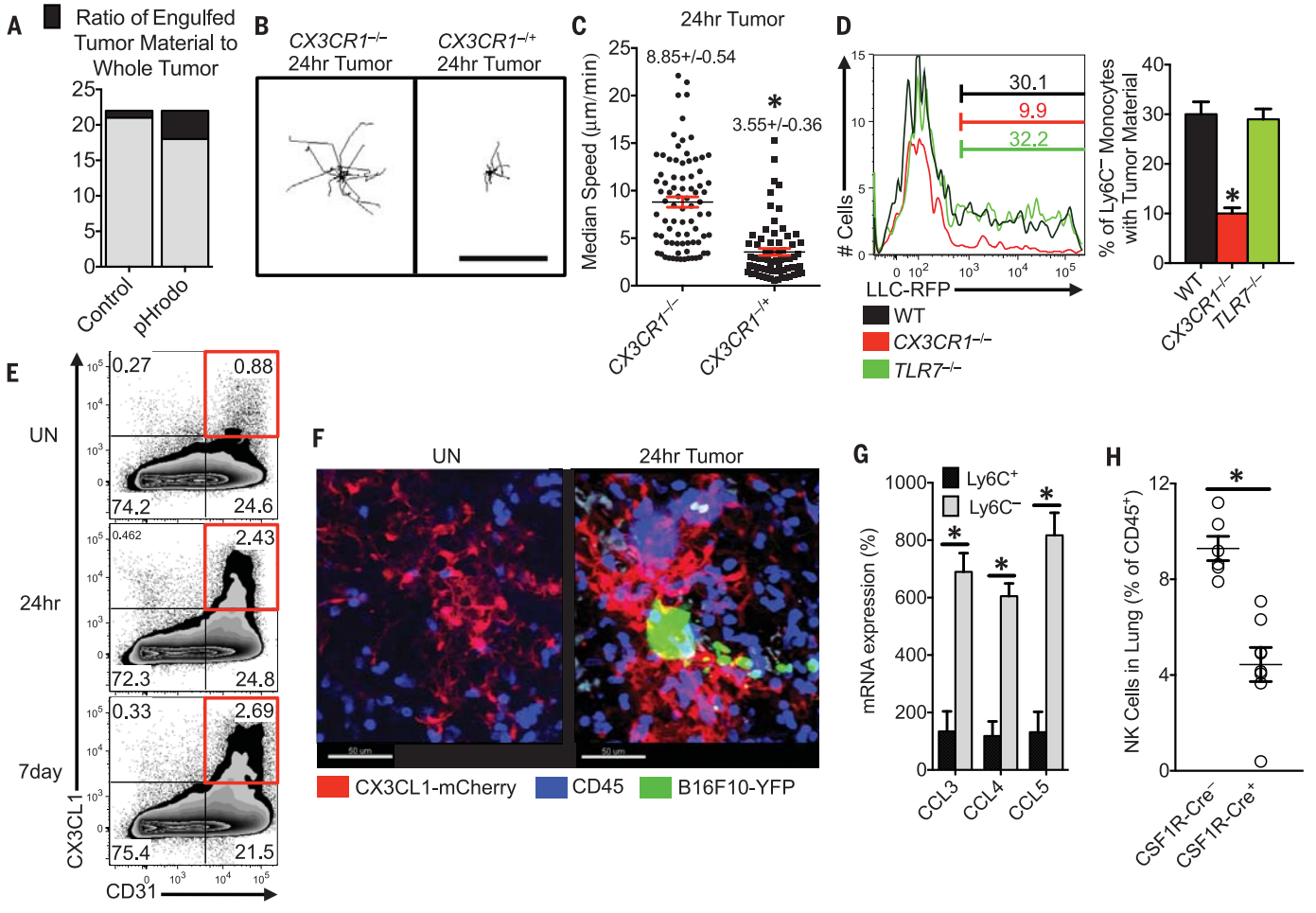

Fig. 4. Patrolling monocytes detect tumor material in a CX3CR1-dependent manner and recruit NK cells to the lung tumor environment. (**A**) Ratio of fluorescent intensity of tumor material engulfed by PMo (black) to fluorescent intensity of whole tumor (black and gray) 3 hours after IV LLC tumor injection. LLC tumors were labeled with either CellTrace Violet control dye (Control) or a pH-sensitive pHrodo Red dye (pHrodo) and then intravenously injected in a 1:1 ratio into a WT mouse (n = 3 mice per group, experiment replicated three times). Representative tracking (**B**) and median speed (**C**) of *Cx3cr1*$^{-/-}$ or *Cx3cr1*$^{-/+}$ monocyte movement 24 hours after IV tumor injection in the lung. Monocyte tracks transposed to a common origin from representative 20-min movies (scale bar, 100 μm; representative tracks are shown from one mouse, median speed was calculated from tumor areas analyzed in three separate mice per group, *P < 0.001). (**D**) (Left) Percentage of Ly6C$^-$ PMo containing LLC-RFP tumor material in the lung 3 hours after IV injection of tumor into representative WT, *Cx3cr1*$^{-/-}$, or *Tlr7*$^{-/-}$ mice. (Right) Quantification of tumor material uptake (n = 3 per group, *P < 0.001 versus WT). (**E**) Percentage of CD31$^+$ CX3CL1$^+$ lung ECs isolated from untreated (UN) mice or from CX3CL1-mCherry mice, 24 hours or 7 days after IV injection of B16F10-YFP tumor cells. (**F**) Representative imaging of CX3CL1-mCherry (red) expression in lung 24 hours after IV injection of B16F10-YFP tumor cells (green) in CX3CL1-mCherry mice. CD45$^+$ immune cells are labeled in blue. (**G**) Relative chemokine mRNA expression in Ly6C$^+$ or Ly6C$^-$ monocytes isolated from lungs by fluorescence-activated cell sorting 24 hours after IV B16F10 tumor injection (monocyte populations isolated from three separate mice; *P < 0.01; experiment repeated three times). (**H**) Percentage of NK cells in the lungs of CSF1R-Cre$^-$*Nr4a1*$^{fl/fl}$ (CSF1R-Cre$^-$) or CSF1R-Cre$^+$*Nr4a1*$^{fl/fl}$ (CSF1R-Cre$^+$) mice 7 days after IV injection of 3 × 10^5 B16F10-luciferase tumor cells (n = 6 mice per group, *P < 0.01). Error bars indicate SEM.

metastasis between WT and CSF1R-Cre^{+}Nr4a1$^{fl/fl}$ mice (fig. S16C). Thus, PMo inhibit metastasis, at least in part, through the regulation of NK cell recruitment and activity.

In summary, we demonstrate that PMo participate in cancer surveillance by preventing tumor metastasis to lung. PMo are actively recruited to lung metastasis sites in a CX3CR1-dependent manner, where they function to scavenge tumor material, as well as to recruit and activate NK cells, leading to the prevention of tumor cell metastasis (fig. S17). Selective targeting by increasing PMo activity and/or their regulation by Nr4a1 may represent a novel therapy for the prevention of cancer metastasis to the lung.

REFERENCES AND NOTES

1. S. K. Biswas, A. Mantovani, *Nat. Immunol.* **11**, 889–896 (2010).
2. P. J. Murray, T. A. Wynn, *Nat. Rev. Immunol.* **11**, 723–737 (2011).
3. T. A. Wynn, A. Chawla, J. W. Pollard, *Nature* **496**, 445–455 (2013).
4. R. A. Franklin *et al.*, *Science* **344**, 921–925 (2014).
5. B. Z. Qian *et al.*, *Nature* **475**, 222–225 (2011).
6. K. Movahedi *et al.*, *Cancer Res.* **70**, 5728–5739 (2010).
7. L. M. Carlin *et al.*, *Cell* **153**, 362–375 (2013).
8. J. Cros *et al.*, *Immunity* **33**, 375–386 (2010).
9. C. Auffray *et al.*, *Science* **317**, 666–670 (2007).
10. R. N. Hanna *et al.*, *Nat. Immunol.* **12**, 778–785 (2011).
11. A. E. Moran *et al.*, *J. Exp. Med.* **208**, 1279–1289 (2011).
12. L. Landsman, S. Jung, *J. Immunol.* **179**, 3488–3494 (2007).
13. L. Landsman, C. Varol, S. Jung, *J. Immunol.* **178**, 2000–2007 (2007).
14. C. Jakubzick *et al.*, *J. Immunol.* **180**, 3019–3027 (2008).
15. C. T. Guy, R. D. Cardiff, W. J. Muller, *Mol. Cell. Biol.* **12**, 954–961 (1992).
16. S. Saeed *et al.*, *Science* **345**, 1251086 (2014).
17. V. Jojic *et al.*, *Nat. Immunol.* **14**, 633–643 (2013).
18. D. E. Sanford *et al.*, *Clin. Cancer Res.* **19**, 3404–3415 (2013).
19. P. Vader, X. O. Breakefield, M. J. Wood, *Trends Mol. Med.* **20**, 385–393 (2014).
20. F. Pucci, M. J. Pittet, *Clin. Cancer Res.* **19**, 2598–2604 (2013).
21. R. N. Hanna *et al.*, *Circ. Res.* **110**, 416–427 (2012).
22. Detailed methods are available as supplementary materials on *Science* Online.
23. G. Thomas, R. Tacke, C. C. Hedrick, R. N. Hanna, *Arterioscler. Thromb. Vasc. Biol.* **35**, 1306–1316 (2015).
24. S. Jung *et al.*, *Mol. Cell. Biol.* **20**, 4106–4114 (2000).
25. F. Geissmann, S. Jung, D. R. Littman, *Immunity* **19**, 71–82 (2003).
26. Y. R. Yu *et al.*, *Int. J. Cancer* **121**, 316–322 (2007).
27. L. Landsman *et al.*, *Blood* **113**, 963–972 (2009).
28. A. I. Su *et al.*, *Proc. Natl. Acad. Sci. U.S.A.* **101**, 6062–6067 (2004).
29. K. W. Kim *et al.*, *Blood* **118**, e156–e167 (2011).
30. J. Zhang, J. M. Patel, *Int. J. Clin. Exp. Med.* **3**, 233–244 (2010).
31. E. Ferretti, V. Pistoia, A. Corcione, *Mediators Inflamm.* **2014**, 480941 (2014).
32. M. Hyakudomi *et al.*, *Ann. Surg. Oncol.* **15**, 1775–1782 (2008).
33. J. Y. Kee *et al.*, *Mol. Clin. Oncol.* **1**, 35–40 (2013).
34. M. H. Park, J. S. Lee, J. H. Yoon, *J. Surg. Oncol.* **106**, 386–392 (2012).
35. A. Schmall *et al.*, *Am. J. Respir. Crit. Care Med.* **191**, 437–447 (2015).
36. M. Tardaguila, S. Manes, "The complex role of chemokines in cancer: The case of the CX3CL1-CX3CR1 axis," in *Oncology: Theory and Practice* (iConcept Press, 2014).
37. E. Romano *et al.*, *Proc. Natl. Acad. Sci. U.S.A.* **112**, 6140–6145 (2015).
38. A. Szaflarska *et al.*, *Exp. Hematol.* **32**, 748–755 (2004).
39. A. A. Maghazachi, *Curr. Top. Microbiol. Immunol.* **341**, 37–58 (2010).
40. M. J. Robertson, *J. Leukoc. Biol.* **71**, 173–183 (2002).

ACKNOWLEDGMENTS

We thank K. Ley and H. Shaked for critically reviewing and editing this manuscript, K. Hogquist for Nr4a1-GFP reporter mice, M. Kronenberg for B16F10 melanoma cells, A. Blatchley and D. Yoakum for assistance with mouse colony management, A. Strasner for help with establishing tumor models, and Z. Mikulski for assistance with imaging. The data presented here are tabulated in the main paper and in the supplementary materials. Nr4a1-floxed conditional mice are available from IGBMC under a material transfer agreement with D.M. and H.I. C.C.H., R.N.H., and the La Jolla Institute for Allergy and Immunology have filed a U.S. patent application (U.S. 13/646,183) that relates to specific topic "Methods and uses of Nur77 and Nur77 agonists to modulate macrophages and monocytes, and treat inflammation, inflammatory disease and cardiovascular disease" and an invention disclosure that relates to the specific topic "Patrolling monocytes control tumor metastasis to the lung." This work was supported by NIH grants R01 HL118765 and R01 CA202987 (both to C.C.H.), American Heart Association Postdoctoral Award 3POST16990029 (to R.T.), NIH F32 postdoctoral fellowship NIH F32 HL117533-02 (to H.N.), American Heart Association Scientist Development Grant 125SDG12070005 (to R.N.H.), the La Jolla Institute for Allergy and Immunology Board of Directors Fellowship (to R.N.H.), CNRS and INSERM (to D.M.), and core funding from SIgN (A*STAR) (to S.K.B.).

SUPPLEMENTARY MATERIALS

www.sciencemag.org/content/350/6263/985/suppl/DC1
Materials and Methods
Figs. S1 to S18
References (*41*–*48*)
Movies S1 to S6

1 July 2015; accepted 2 October 2015
Published online 22 October 2015
10.1126/science.aac9407